Original Article

대한치과재료학회지 48(3) : 191-210, 2021
Korean Journal of Dental Materials (*Korean J Dent Mater*)
ISSN:2384-4434 (Print); 2384-3268 (Online)
Available online at http://www.kadm.org
http://dx.doi.org/10.14815/kjdm.2021.48.3.191

치과임플란트용 Ti-Ta-Ag-Pt 합금에 형성된 나노튜브의 표면특성

김승표, 최한철*

조선대학교 치과대학 치과재료학교실

Surface characteristics of nanotube-formed Ti-Ta-Ag-Pt alloys for dental implants

Seung-Pyo Kim, Han-Cheol Choe*

Advanced Functional Surface & Biomaterials Research Lab, Department of Dental Materials & Research Center of Nano-Interface Activation for Biomaterials, College of Dentistry, Chosun University Gwangju, Republic of Korea

본 연구에서는 나노튜브로 형성된 치과 임플란트용 Ti-Ta-Ag-Pt 합금의 표면 특성을 조사하였다. 이를 위하여 Ti-xTa-2Ag-2Pt합은 Ta 함량을 10, 30 및 50 wt%로 변화하여 진공 아크 용해로를 사용하여 제조한 다음, 1050 ℃에서 1시간 동안 열처리한 후 균질화처리하였다. Ti-xTa-2Ag-2Pt(x = 10-50 wt%) 합금의 나노튜브 형성은 1.0 M H_3PO_4 + 0.8 wt% NaF 전해액에서 30 V의 DC 전원을 사용하여 수행하였다. 광학 현미경(OM), 전계 방출 주사 전자 현미경(FE-SEM), 에너지 분산형 X선 분광법(EDS), X-선 회절법(XRD), 젖음성 및 나노 압입 시험을 통하여 표면특성을 조사하였다. 그 결과 다음과 같은 결론을 얻었다. Ti-xTa 합금의 미세조직은 α"상(Widmanstätten 구조)과 β상 등축 구조로 구성되었으며 α상의 XRD 피크는 Ta 함량이 증가함에 따라 낮아지고 β상의 XRD 피크는 증가하였다. Ti-30Ta-2Ag-2Pt 합금의 탄성계수는 다른 합금보다 낮게 나타났다. Ti-10Ta-2Ag-2Pt 및 Ti-30Ta-2Ag-2Pt 합금에서 규칙화된 나노튜브의 배열을 보였다. Ti-50Ta-2Ag-2Pt 합금에서 나노 입자가 발견되었으며 Ta 함량이 증가함에 따라 크고 작은 나노튜브의 직경이 각각 증가 및 감소하였다. 나노튜브는 바늘과 같은 구조를 갖는 Widmanstätten상에서 성장하지 않았고 또한 결정립계에서도 나노튜브가 형성되지 않았다. TiO_2의 아나타제상은 Ti-30Ta-2Ag-2Pt 합금에서 나타났고 Ti-50Ta-2Ag-2Pt 합금에서 사라졌다. 나노튜브로 형성된 Ti-30Ta-2Ag-2Pt 합금의 접촉각은 다른 합금보다 작게 나타났다.

색인단어 : Ti-xTa-2Ag-2Pt 합금, 나노튜브, 탄성계수, α 및 β 상, 접촉각

Seung-Pyo Kim (ORCID: 0000-0002-5618-2902)

*Correspondence: Han-Cheol Choe (ORCID: 0000-0003-1966-781x)
309 Poongmoon-daero, Gwangju 61452, Republic of Korea
Affiliation: Advanced Functional Surface & Biomaterials Research Lab, Department of Dental Materials & Research Center of Nano-Interface Activation for Biomaterials, College of Dentistry, Chosun University, Gwangju, Republic of Korea.
Tel: +82-62-230-6896, Fax: +82-62-230-6896
E-mail: hcchoe@chosun.ac.kr

Received: Sep. 03, 2021; Revised: Sep. 27, 2021; Accepted Sep. 28, 2021

Introduction

Titanium (Ti) and Ti-6Al-4V alloys are excellent metallic medical materials because of their excellent combination of mechanical properties, corrosion resistance, and biocompatibility, and are widely used in dental and orthopedic implants (1). However, the Ti-6Al-4V alloy stimulates inflammation and osteolysis of the implant due to the toxicity of stimulation caused by the influence of Al and V ions, which lead to the resorption of adjacent bone tissues due to the large difference in elasticity modulus between the implant and the adjacent bone tissues (2). The ideal biomedical implant materials should have excellent biocompatibility, high strength, good corrosion resistance, and low elastic modulus, similar to human bones (3, 4). In addition, because the Ti alloy has no antibacterial action, it is difficult to treat implant-associated bacterial infections (5). To overcome these disadvantages, many other Ti alloys have been developed that have a low modulus of elasticity, such as non-toxic elements of Ta, Zr, Nb, Mo, and Hf, which are harmless to the human body (4). In particular, Ta has similar chemical properties to glass and is immune to attack from almost all acids except concentrated HF (6). In addition, Ti-Ta alloys are attracting attention for their excellent corrosion resistance due to oxide films of TiO_2 and Ta_2O_5 (7). Silver is much stronger than Cu and has a broad spectrum of antimicrobial activity, and a small amount of Ag can lead to a very strong antimicrobial effect. It is also reported that the addition of an appropriate concentration of Ag improves the strength and grindability of the titanium alloy while maintaining high elongation and reducing the modulus of elasticity (8). It has been reported that Pt is more active in the galvanic series than Ag, and thus significantly enhances the Ag antibacterial effect due to galvanic action (9).

Among the surface modification techniques used to improve the bioactivity of dental implants, titanium anodization has attracted considerable interest. TiO_2 nanotubes are especially important because of their unique physical and chemical properties that can be used in a variety of applications (10). The nanostructured surface was prepared by anodizing a fluoride-containing electrolyte, such as $(NH_4)_2SO_4$-NH_4F mixture, chromic acid-HF mixture, HF, H_2SO_4-HF mixture, and H_3PO_4-NaF mixture, to form self-organized nanotubes of TiO_2 (11–13). When titanium oxide nanotubes are formed on the surface of titanium alloy, adhesion and cell attachment are greatly improved and bone fusion is improved (14). Electrochemical anodization seems to be a relatively straightforward way to convert titanium implant surfaces into nanostructures (15). However, there is little research on the surface treatment of alloys with added Pt and Ag, which have antibacterial action, low modulus of elasticity, and non-toxic elements that are harmless to the human body.

Therefore, in this study, the surface characteristics of nanotube-formed Ti-Ta-Ag-Pt alloys for dental implants were researched using various experimental instruments.

Materials and Methods

In this study, Ti-xTa-2Ag-2Pt quaternary alloys used were prepared from pure Ti (G&S Titanium, Grade 4, USA), Ta (99.95% purity, Kurt J. Lesker Company, USA), Ag (99.99% purity, iTASCO company, Korea), and Pt (99.99% purity, iTASCO company, Korea) with Ta content of 10, 30, and 50 wt%. Each alloy was melted 6 times using a vacuum arc-melting furnace (Model MSTF-1650, MS Eng., Korea) under a high-purity argon atmosphere to improve alloy homogenization. The alloy was homogenized by heat treatment at 1050 ℃ for 1 h in a high-purity argon atmosphere and followed by quenching in 0 ℃ water. For the experiments, each sample was first cut to a 3-mm thickness using a high-speed

diamond-cutting machine (Accutom-5, Struers, Denmark) at a speed of 2000 rpm. Samples of 3-mm thickness were polished with 100–2000 grit sand paper and then polished with 0.3-μm Al_2O_3 slurry. The polished samples were ultrasonically cleaned in deionized water and dried in flowing nitrogen. The nanotube formation on Ti-xTa-2Ag-2Pt (x = 10–50 wt%) alloy was performed using a DC power source (Agilent E3641 A, USA) as a two-electrode system, using platinum as a counter electrode and a working electrode as an anode. All the nanotube formations were anodized at room temperature for 2 h with a DC power supply of 30 V in 1.0 M H_3PO_4 + 0.8 wt% NaF electrolyte solution. After the experiment, the sample surface was washed with ethanol and distilled water and air dried. The Ti-xTa-2Ag-2Pt alloy was chemically etched in a Keller's solution (190 mL H_2O + 3 mL HCl + 5 mL HNO_3 + 2 mL HF) and then an optical microscope (OM, Olympus BM60M, Japan) was used to observe the microstructure. The surface morphology and structural characterization of the samples after nanotube formation was carried out with field-emission scanning electron microscopy (FE-SEM, Hitachi 4800, Japan), which was also capable of energy-dispersive X-ray spectroscopy (EDS) analysis. The phases were identified by X-ray diffraction (XRD) using a diffractometer (X'pert PRO, Philips, Netherlands) and Cu Kα radiation (λ = 1.54060 nm). The diffraction peaks from the atomic planes were compared to files from the Joint Committee on Powder Diffraction Standards (JCPDS). The elastic modulus and Vickers hardness of the Ti-xTa-2Ag-2Pt alloys were measured three times for each samples using a nano-indentation tester with an allowable load range of 500 mN, pulling speed of 10 N/min, fine depth range of 40 μm, and large depth range of 200 μm (TTX-NHT3, Anton Paar, Austria). The surface roughness of the samples was measured by using a surface roughness tester (Surfcorder SE 1700, Kosaka Lab. Ltd., Japan) and measured using a probe method. The measurement speed was set to 0.500 mm/s and the measurement length was set to 4.000 mm. The surface wettability test was performed on the surface and anodized surface using a water contact-angle goniometer (Kruss DSA100, Germany) in distilled water-drop mode with 6-μL drops. The contact angles were measured by the sessile droplet method with the help of a contact angle meter, which contains an automatic drop-deposition system and video camera.

Results and Discussion

Fig. 1 shows the microstructure of Ti-xTa and Ti-xTa-2Ag-2Pt alloys with Ta content of 10, 30, and 50 wt%. Fig. 1 (a) to (c) show the optical micrographs (OM) for Ti-xTa alloys, and (d) to (f) show the OM results for Ti-xTa-2Ag-2Pt alloys. In Fig. 1 (a) to (c), the microstructure of the Ti-xTa alloy has an α',α''-phase which are needle-like structures and a β-phase of equiaxed structure. As the Ta content increases, the martensite α' and α'' phase gradually disappears and only the equiaxed structure appears. In the previous study on Ti-Ta alloys, the orthorhombic (α'') martensite was observed for high Ta contents ranging from 26 to 52 wt%. When the Ta content exceeds 65% by weight, there is a single β phase, quasi-stable body-centered cubic (bcc), or orthorhombic (α'') martensite structure (3). As shown in Fig. 1 (d), the microstructure of the Ti-xTa-2Ag-2Pt alloy shows properties similar to those of the Ti-xTa alloy; the Ti-50Ta-2Ag-2Pt alloy did not have a martensitic structure and showed only complete equiaxed structure. It is considered that Ta, which is a stabilizing element in the Ti alloy, modifies the martensitic starting deformation temperature due to the influence of Ag and Pt alloys. In a previous study (16), it was reported that, in the case of an alloy containing 2.0–4.0 wt% silver, the formation of the acicular α-phase was observed inside the β-phase, and the acicular phase became thinner with

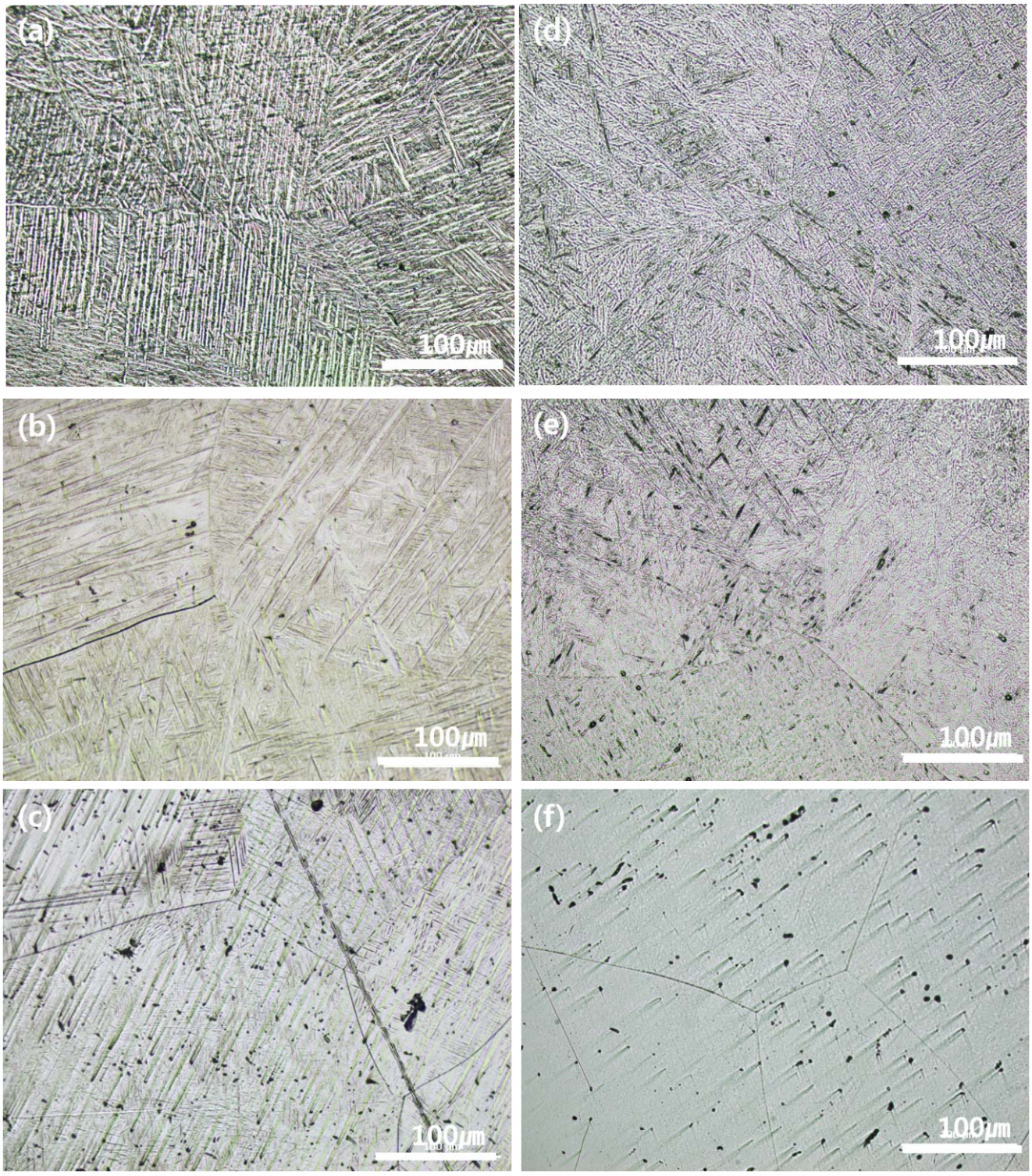

Figure 1. OM images of Ti-xTa-2Ag-2Pt alloys after heat treatment at 1050 ℃ for 1 h in Ar atmosphere, followed by 0 ℃ water quenching: (a) Ti-10Ta alloy, (b) Ti-30Ta alloy, (c) Ti-50Ta alloy, (d) Ti-10Ta-2Ag-2Pt alloy, (e) Ti-30Ta-2Ag-2Pt alloy, and (f) Ti-50Ta-2Ag-2Pt alloy.

increasing silver content. In Fig. 1 (a) and (d), the thickness of the needle-like structure may be thinned by the addition of Ag and Pt, which is consistent with the results reported in the paper (16). The addition of a small amount of Pt was found to significantly improve the antimicrobial performance of Ag. For this reason, it is thought that the addition of Pt affects the microstructure by the active formation of Ag ions (9, 17).

Fig. 2 shows an FE-SEM image showing the microstructure of Ti-xTa and Ti-xTa-2Ag-2Pt alloys with Ta contents of 10, 30, and 50 wt%. Fig. 2 (a) to (c) show the FE-SEM images for Ti-xTa alloys, and (d) to (f) show FE-SEM images for Ti-xTa-2Ag-2Pt alloys. As shown in the OM image in Fig. 1, Ti-xTa alloy and Ti-xTa-2g-2Pt alloy showed a Widmanstätten structure (18) with a fine orthorhombic structure, as shown in Fig. 2 (a, b, d), and an equiaxed structure, as shown in Fig. 2(e, f), and the morphology of the microstructure changed with increasing Ta content. In Fig. 2 (c) and (e), we can observe that a Widmanstätten-type microstructure that is slightly different from the OM analysis results; the grain boundaries are observed. This is considered to be because the α'' structure is very finely distributed or the etching treatment is slightly less. However, when Ag and Pt are added, the needle-like structure is greatly thinned and disappears, as shown in Fig. 2 (e and f).

Fig. 3 shows the XRD pattern of the Ti-xTa-2Ag-2Pt alloy. The β-phase and α-phase peaks were detected at all peaks in the case of Ti-xTa-2Ag-2Pt alloy (x = 10, 30, and 50 wt%). As the Ta content increased, the α-phase peak decreased and the β-phase peak increased. It is clear that the β-volume fraction of the alloy increases because tantalum is the β-stabilizer element of the titanium alloy (19). The martensite structure of the α-phase peak appears at 2θ = 34°, 39°, 40°, 52°, and 76°, and the equiaxed structure of the β-phase peak appears at 2θ = 38°, 56°, and 70°. These peaks show similar results to those observed in the microstructure, as shown in Fig. 1 and Fig. 2. Moreover, no distinct diffraction peaks due to the addition of Ag and Pt were observed. It is considered that the Ti_2Ag and Ti_3Pt (20) phases of a small amount of alloy were completely dissolved due to the homogenization treatment (8).

Fig. 4 shows the results of nano-indentation test for measuring the elastic modulus and Vickers hardness. As shown in the graph, the Ti-30Ta-2Ag-2Pt alloy was found to be shifted to the right in the load–displacement graph, and the elastic modulus was also the lowest among the alloys at 72.10 GPa. When 30% of Ta is added to Ti, the elastic modulus reaches its minimum as the β structure is formed, and when Ta is increased again, other phases, such as ω phase, appear and increase the elastic modulus (3). The elastic modulus of the Ti-xTa-2Ag-2Pt alloy is much lower than that of the conventional CP Ti and Ti-6Al-4V alloys (about 125 GPa), and can reduce the stress-shielding effect (21). The addition of an appropriate concentration of Ag is believed to improve the strength and grindability of the titanium alloy while maintaining a high elongation and reducing the modulus of elasticity (8).

There are several reports on the elastic modulus of the various stages of titanium alloys. The ω phase has the highest elastic modulus, the elastic modulus of the α'' phase is lower than that of the α' phase, and the β phase has the lowest elastic modulus (3, 22). It is well known that the elastic modulus, one of the intrinsic natures of materials, is determined by the bonding force among atoms. This bonding force is not only related to the crystal structure, but also to the distances among atoms, and it can be affected by alloying addition, heat treatment, and plastic deformation (22). The elastic modulus mainly depends on the chemical composition, that is, it is sensitive to the Ta content (3). It is believed that the titanium alloy can bring about a stabilized β-Ti structure and an antibacterial effect due to the presence of Ta, Ag, and Pt. The highest Vickers hardness value was 556 HV for

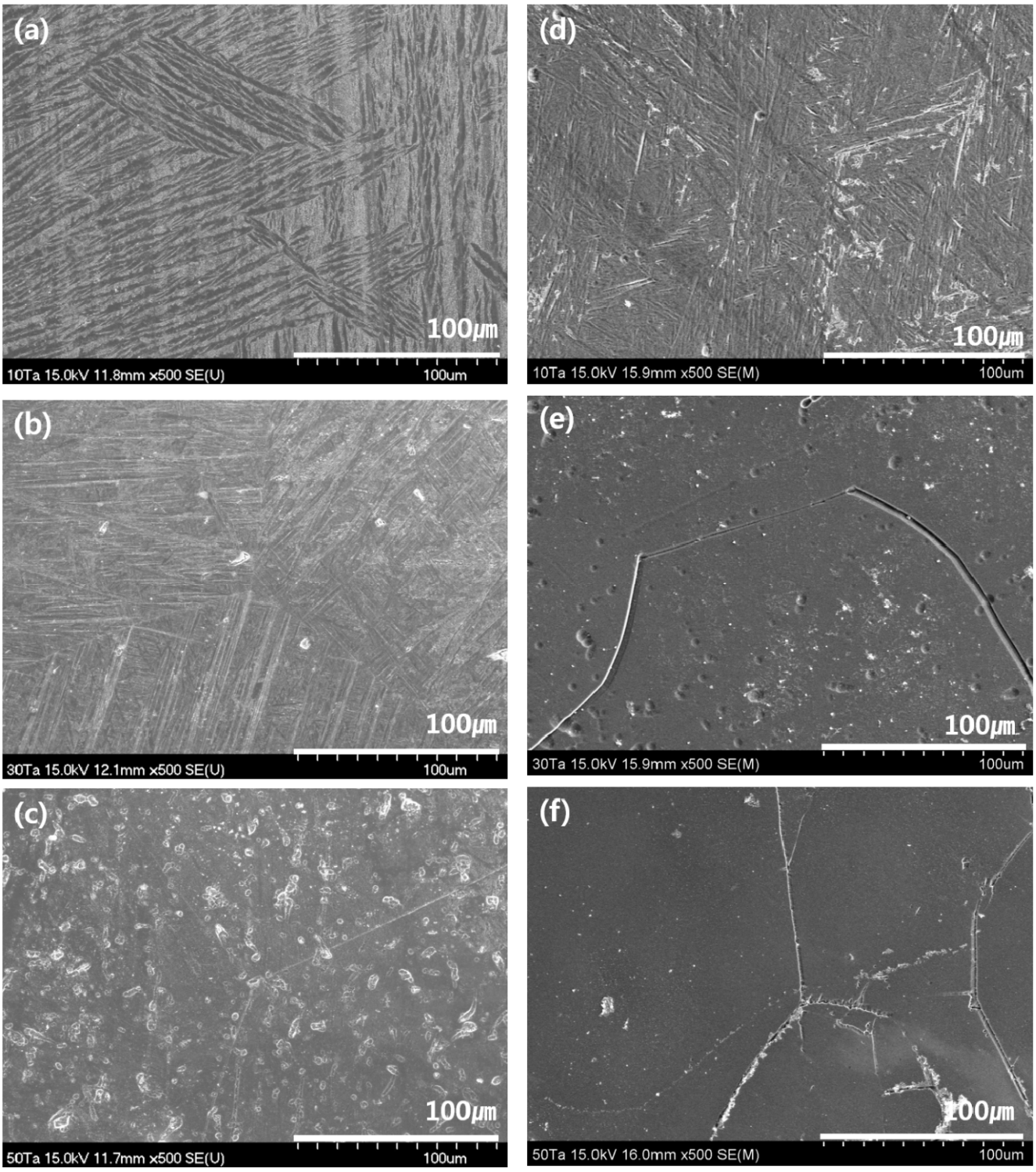

Figure 2. FE-SEM images of Ti-xTa-2Ag-2Pt alloys after heat treatment at 1050 ℃ for 1 h in Ar atmosphere, followed by 0 ℃ water quenching: (a) Ti-10Ta alloy, (b) Ti-30Ta alloy, (c) Ti-50Ta alloy, (d) Ti-10Ta-2Ag-2Pt alloy, (e) Ti-30Ta-2Ag-2Pt alloy, and (f) Ti-50Ta-2Ag-2Pt alloy.

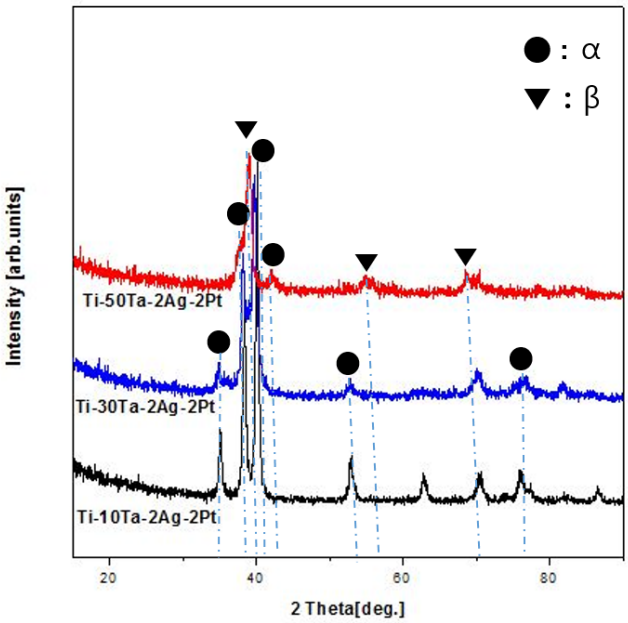

Figure 3. XRD patterns for the homogenized Ti-xTa-2Ag-2Pt alloys.

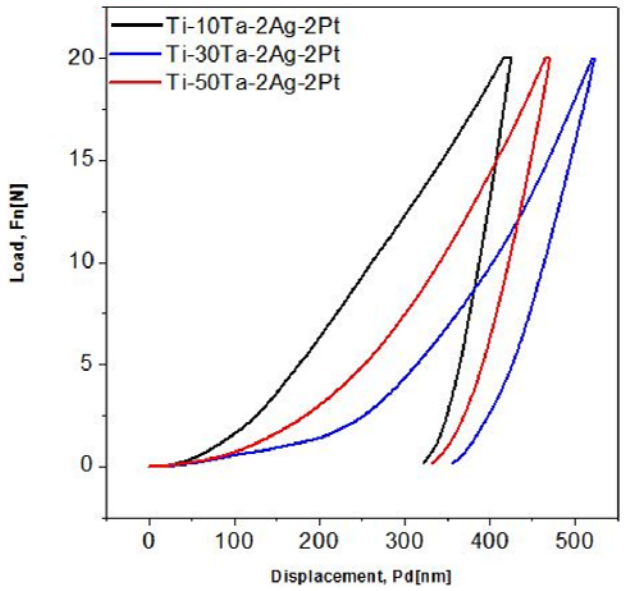

Figure 4. Load-displacement graphs of Ti-xTa-2Ag-2Pt alloys from nano-indentation test.

Ti-10Ta-2Ag-2Pt alloy and 399 HV for Ti-50Ta-2Ag-2Pt alloy.

The surface hardness of Ti-xTa and Ti-xTa-2Ag-2Pt alloys was found to increase with the increasing needle-like structure (Widmanstätten) and decrease with the formation of the β-phase. It is believed that this is due to the internal stress generated by the formation of the martensite structure (23). The elastic modulus and Vickers hardness values are shown in Table 1.

Table 1. The elastic modulus and Vickers hardness value of Ti-xTa-2Ag-2Pt alloys.

Specimens	Properties	
	Elastic modulus (GPa)	Vickers hardness (Hv)
Ti-10Ta-2Ag-2Pt	142.04	556.07
Ti-30Ta-2Ag-2Pt	72.10	426.45
Ti-50Ta-2Ag-2Pt	87.07	399.58

Fig. 5 shows FE-SEM image of the nanotube morphology of Ti-xTa and Ti-xTa-2Ag-2Pt alloys in the 1.0 M H_3PO_4 + 0.8 wt% NaF electrolytes for 2 h at an applied potential of 30 V. Fig. 5 (a-c) shows the top morphologies of nanotube on Ti-xTa alloy with 30000× magnifications and Fig. 5 (d-f) shows the top morphologies of the nanotube on Ti-xTa-2Ag-2Pt alloy with 30000× magnification. The Ti-10Ta and Ti-30Ta alloy nanotubes in Fig. 5 (a) and (b), respectively, show clearly formed nanotubes on the surface, and Ti-50Ta in Fig. 5 (c) shows the formation of nanoparticles. In the Ti-xTa-2Ag-2Pt alloy shown in Fig. 5 (d-f), the formation of highly arrayed nanotubes can be observed only in the Ti-10Ta-2Ag-2Pt and Ti-30Ta-2Ag-2Pt alloys shown in Fig. 5 (d-e); the shape of the nanoparticles was seen in the Ti-50Ta-2Ag-2Pt alloy. The Ti-10Ta-2Ag-2Pt, Ti-30Ta-2Ag-2Pt, and Ti-50Ta-2Ag- 2Pt alloys showed a similar appearance to the conventional Ti-xTa alloys. The average diameters of the large and small nanotubes are (a) 180 nm and

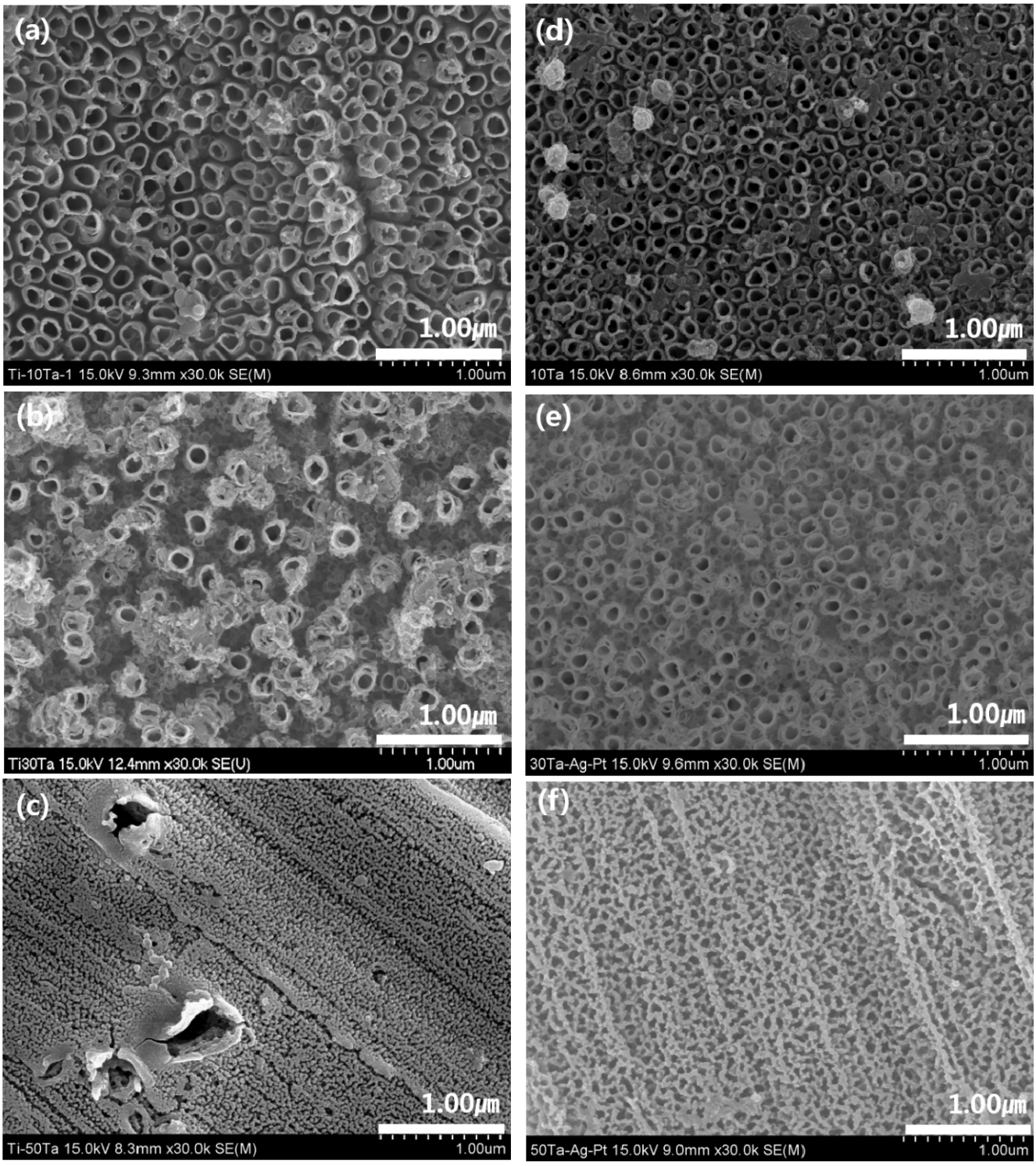

Figure 5. FE-SEM micrographs showing views of the surfaces of the nanotube layers formed on the Ti-xTa and Ti-xTa-2Ag-2Pt alloys in 1.0 M H3PO4 with 0.8 wt. % NaF electrolyte after anodization for 2 h at 30V : (a) : Ti-10Ta, (b) : Ti-30Ta, (c) Ti-50Ta, (d) Ti-10Ta-2Ag-2Pt, (e) Ti-30Ta-2Ag-2Pt, and (f) Ti-50Ta-2Ag-2Pt.

105 nm, (b) 200 nm and 95 nm, (c) 160 nm and 97 nm, (d) 138 nm and 99 nm, (e) 179 nm and 99 nm, and (f) 151 nm and 93 nm, respectively. It is indicated that the nanotubes in the Ti-xTa-2Ag-2Pt alloy were slightly smaller than those in the Ti-xTa alloy. Moreover, the dissolution rate of the oxide layer depends on the metallic phases of substrate. For this reason, it is considered that the growth is slowed by the slow attack of fluoride ions on the oxide film containing Ag and Pt, although the influence of Ta is large (13). As shown in Figs. 5 (c) and 5 (f), the β phase is present in the dented part and the nanopore is formed in the flat part where the α phase is present. An unstable phase, such as α'', can be easily dissolved in fluoride solution, whereas the stable β phase is difficult to dissolve in this solution (24).

From the surface roughness analysis, the arithmetic mean roughness (Ra) values of the Ti-xTa-2Ag-2Pt alloy were 0.060, 0.077, and 0.120, respectively. The Ra values of the Ti-xTa-2Ag-2Pt alloy after nanotube formation were 0.585, 0.473, and 0.180, respectively, as shown in Table 2. The surface of the nanotubes has high roughness because the surface is etched by the fluorine ions, and the tendency to decrease as the Ta content increases is because the texture changes to the α phase to the β phase. It is considered that the case where the β phase is mixed becomes rougher than the case where only the β phase exists. In addition, it is thought that the roughness is decreased due to uniform etching on the surface, as shown in Fig. 1. The Ti-xTa-2Ag-2Pt alloy after nanotube formation is probably affected by the irregular and regular structure of the surface according to crystal structures.

Fig. 6 shows the FE-SEM image of bottom view of nanotube-formed Ti-xTa-2Ag-2Pt alloys in the 1.0 M H_3PO_4 + 0.8 wt% NaF electrolytes for 2 h at an applied potential of 30 V. Fig. 6 (a–c) shows the low-magnification image and Fig. 6 (d–f) shows the high-magnification image. To analyze the size of the nanotubes more accurately, we used an image analyzer (Image J, Wayne Rasband, USA) to measure the number and diameter of large and small nanotubes in a high-magnification image of the nanotube bottom. The measured data are shown in Table 3. As shown in Table 3, the nanotube diameter increases slightly, the number of small nanotubes gradually decreases, and a large number of large nanotubes are formed as the Ta content increases. In Fig. 6, it can be seen that as the Ta content increases, the area of the small and large nanotubes becomes wider. These phenomena were indicate that Ta has a role in the formation of a stable oxide film that protects the alloy surface from fluoride ion attack, and that areas devoid of nanotubes act as subsequent nucleation sites for the smaller tubes (25). The Ti-50Ta-2Ag-2Pt alloy in Fig. 6 (c) shows two regions: dark and bright. This shows that the nanotube layer grew at different rates. The nanotube diameter of the Ti alloy depends on TiO_2 and Ta_2O_5, and various nanotube diameters can be achieved. Therefore, nanotube regulation can be controlled by the Ta content (26).

Fig. 7, Fig. 8, and Fig. 9 show FE-SEM images of the

Table 2. The surface roughness value of Ti-xTa-2Ag-2Pt alloys.

Surface roughness (μm)	Specimens					
	Ti-10Ta-2Ag-2Pt	Ti-30Ta-2Ag-2Pt	Ti-50Ta-2Ag-2Pt	Nanotube+ Ti-10Ta-2Ag-2Pt	Nanotube+ Ti-30Ta-2Ag-2Pt	Nanotube+ Ti-50Ta-2Ag-2Pt
Ra(μm)	0.060 (±0.013)	0.077 (±0.009)	0.120 (±0.073)	0.585 (±0.246)	0.473 (±0.05)	0.180 (±0.024)

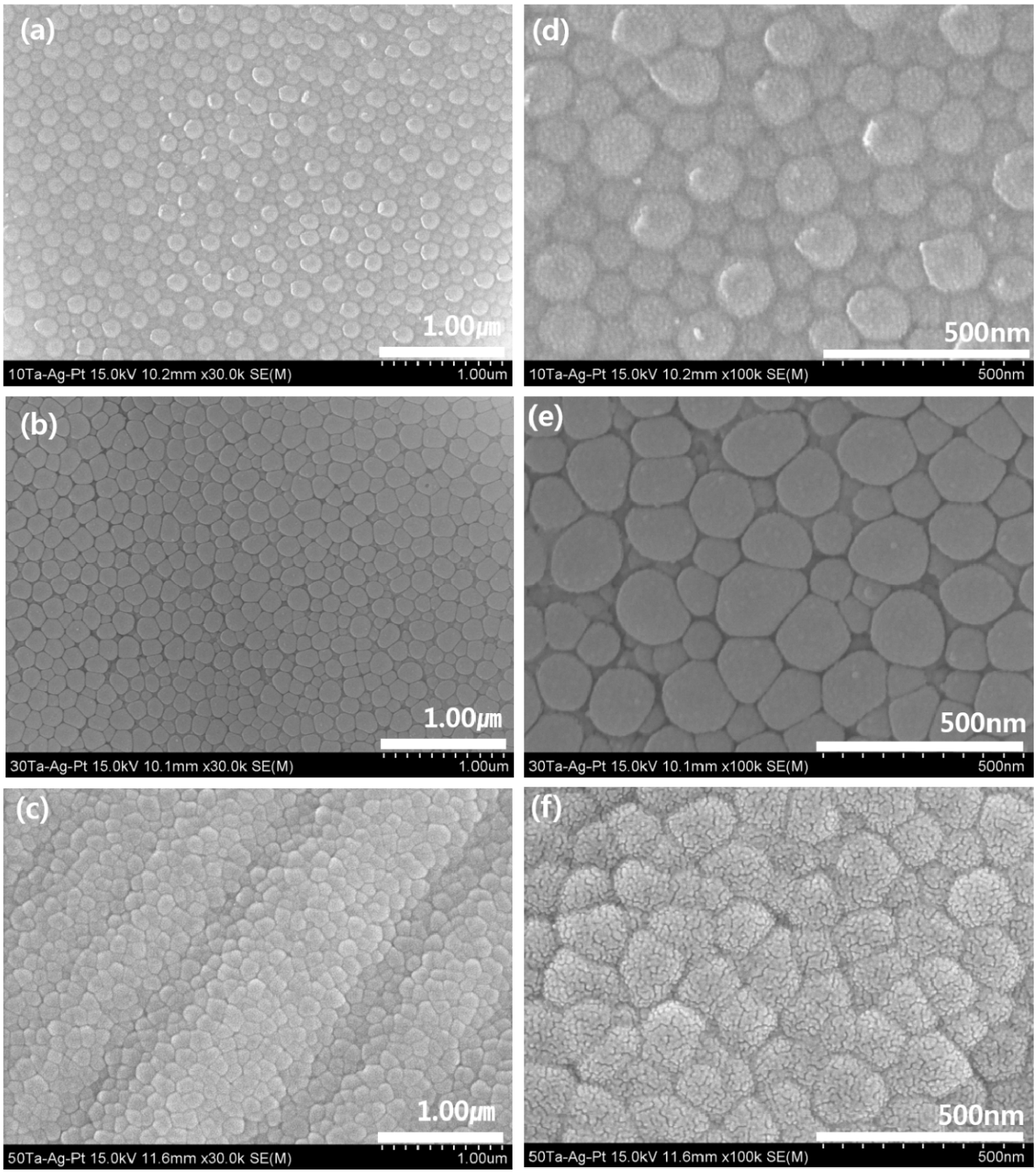

Figure 6. FE-SEM micrographs showing views of the bottom of the nanotube layers formed on the Ti-xTa-2Ag-2Pt alloys in 1.0 M H3PO4 with 0.8 wt. % NaF electrolyte after anodization for 2 h at 30V : (a) Ti-10Ta-2Ag-2Pt at low magnification, (b) Ti-30Ta-2Ag-2Pt at low magnification, (c) Ti-50Ta-2Ag-2Pt at low magnification, (d) Ti-10Ta-2Ag-2Pt at high magnification, (e) Ti-30Ta-2Ag-2Pt at high magnification, and (f) Ti-50Ta-2Ag-2Pt at high magnification.

Table 3. The diameter and number of nanotube of Ti-xTa-2Ag-2Pt alloys.

Specimens	Nanotube diameter (nm)		Numbers of nanotube (N/μm^2)	
	Large	Small	Large	Small
Ti-10Ta-2Ag-2Pt	138.3(±6.5)	99.4(±8.4)	20	58
Ti-30Ta-2Ag-2Pt	179.8(±14.7)	99.8(±10.1)	23	28
Ti-50Ta-2Ag-2Pt	158.9(±17.9)	110.6(±10.9)	30	16

Figure 7. FE-SEM micrographs showing views of the microstructure surfaces of the nanotube layers formed on the Ti-10Ta-2Ag-2Pt alloys in 1.0 M H_3PO_4 with 0.8 wt. % NaF electrolyte after anodization for 2 h at 30V : (a) : ×500, (b) : ×8,000, (c) ×10,000, (d) ×25,000.

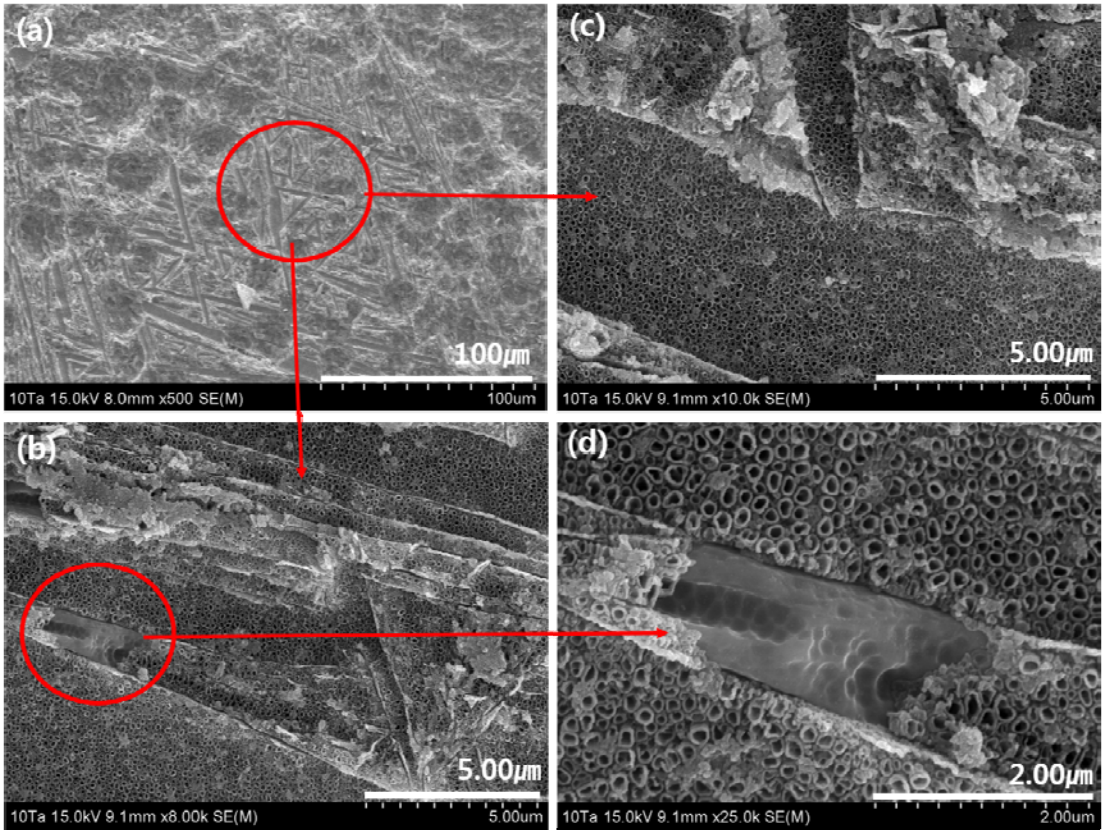

microstructure surfaces on nanotube-formed Ti-xTa-2Ag-2Pt alloys in the 1.0 M H_3PO_4 + 0.8 wt% NaF electrolytes for 2 h at an applied potential of 30 V. As shown in Fig. 7 and Fig. 8, nanotubes grown on the grain boundaries can be observed in the nanotubes formed on the Ti-10Ta-2Ag-2Pt and Ti-30Ta-2Ag-2Pt alloys. In the Ti-10Ta-2Ag-2Pt alloy of Fig. 7, the non-uniform surface of the oxide layer can be observed in Fig. 7 (b) in the direction of the arrow in the low-magnification image of Fig. 7 (a). Fig. 7 (c) shows the formation of uniform nanotubes. Fig. 7 (d) shows that the nanotubes did not grow in a needle-like structure (Widmanstätten). This is

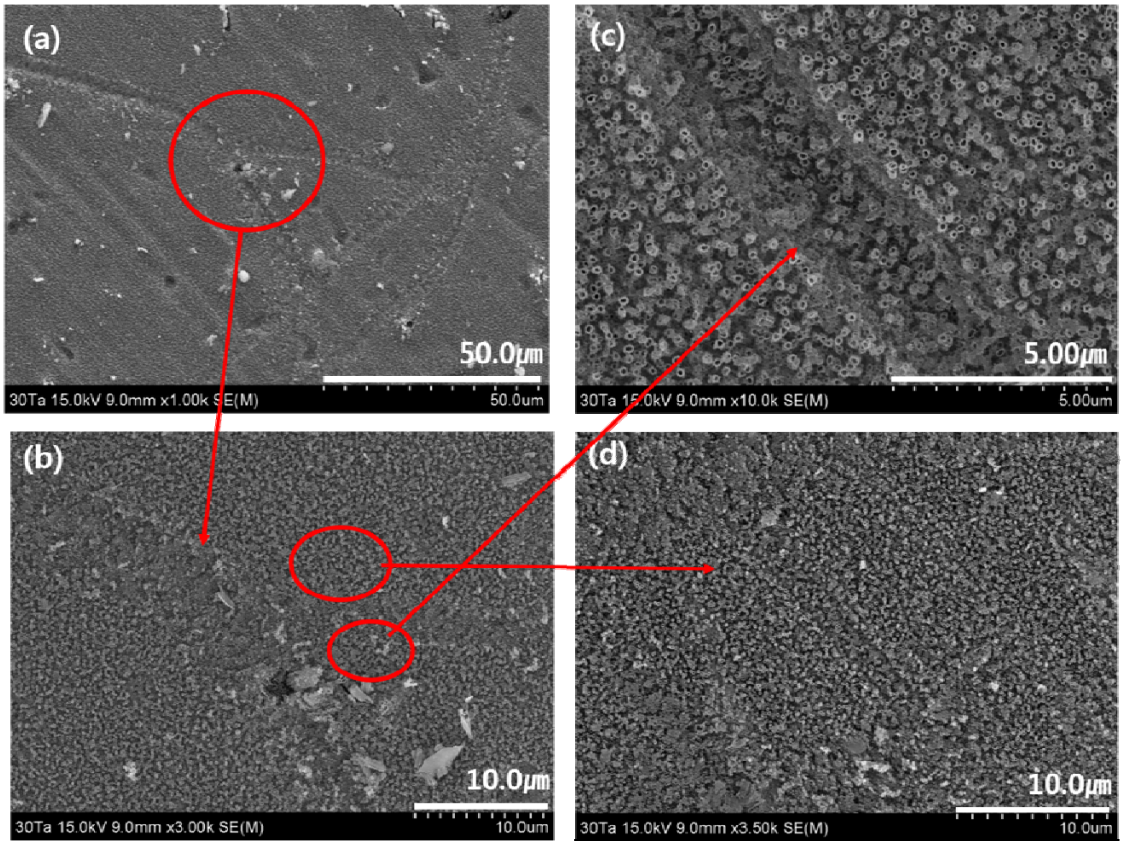

Figure 8. FE-SEM micrographs showing views of the microstructure surfaces of the nanotube layers formed on the Ti-30Ta-2Ag-2Pt alloys in 1.0 M H_3PO_4 with 0.8 wt. % NaF electrolyte after anodization for 2 h at 30V : (a) : ×1,000, (b) : ×3000, (c) ×10,000, (d) ×3,500.

thought to be due to the α phase of the needle-like structure with internal stress, as observed in Fig. 1 and Fig. 2.

The Ti-30Ta-2Ag-2Pt alloy in Fig. 8 confirmed that the nanotubes were formed on both grain boundaries and surfaces, as shown by the arrows, and it was confirmed that the Ti-30Ta-2Ag-2Pt alloy was divided into two disordered structures. It can be seen that nanotubes are not formed at the grain boundaries by fluoride ions, and the grain boundaries are heavily corroded, especially at the edges. This is because the grain boundary is unstable, compared to the matrix. It is believed that some grain boundaries are more etched than others are because oxidation and dissolution reactions take place during nanotube growth (27). In the Ti-50Ta-2Ag-2Pt alloy of Fig. 9, nanotubes were not observed, only nanoparticles. This is because the nanoporous layer is formed on the surface, and the nanotube layer then grows below the nanoporous layer. At this stage, the tube begins to grow at different rates due to alloying elements, such as Ta, Ag, and Pt, and may be different in the α phase or β phase (18). It can be seen that the growth behavior of nanotubes can be affected by the microstructure.

Fig. 10 shows the EDS mapping image of cross-sectioned nanotubes of Ti-xTa-2Ag-2Pt alloys in 1 M H_3PO_4 + 0.8 wt% NaF electrolytes for 2 h at an applied potential of 30 V. Fig. 10 (a) is a cross-sectional image of Ti-30Ta-2Ag-2Pt alloy after nanotube formation, and

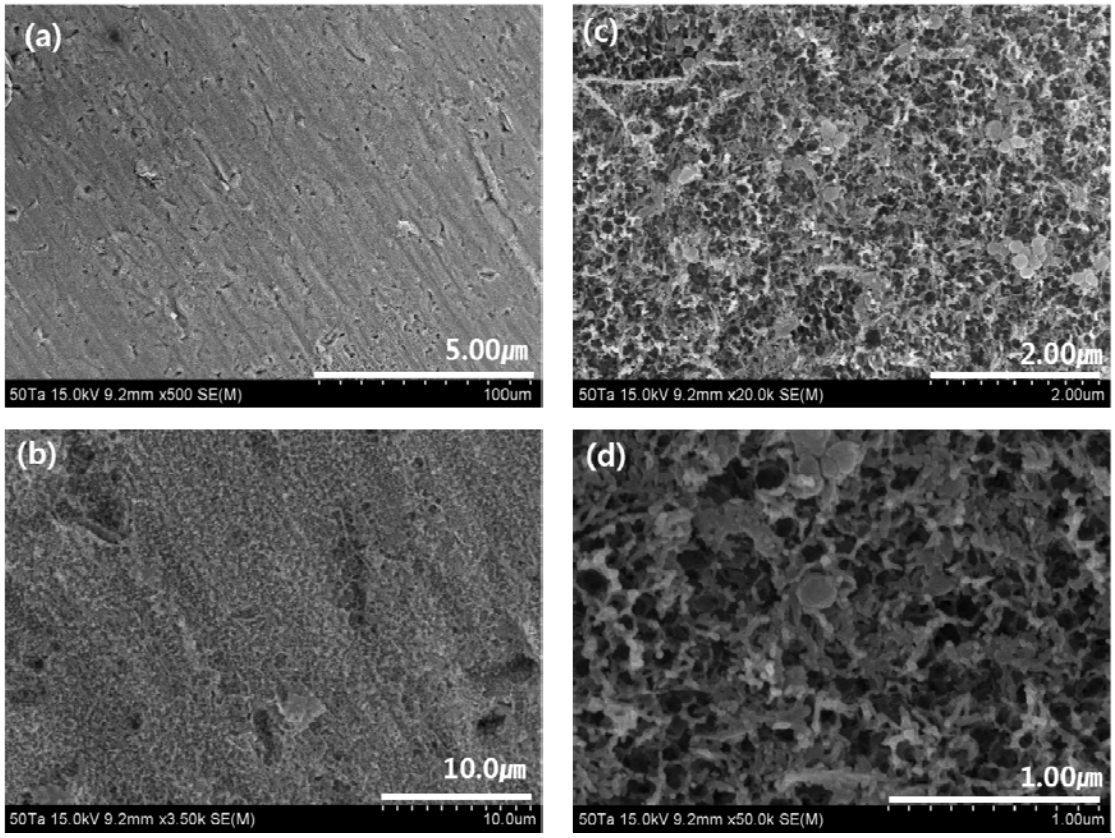

Figure 9. FE-SEM micrographs showing views of the microstructure surfaces of the nanotube layers formed on the Ti-50Ta-2Ag-2Pt alloys in 1.0 M H_3PO_4 with 0.8 wt. % NaF electrolyte after anodization for 2 h at 30V : (a) : ×500, (b) : ×3,500, (c) ×20,000, (d) ×50,000

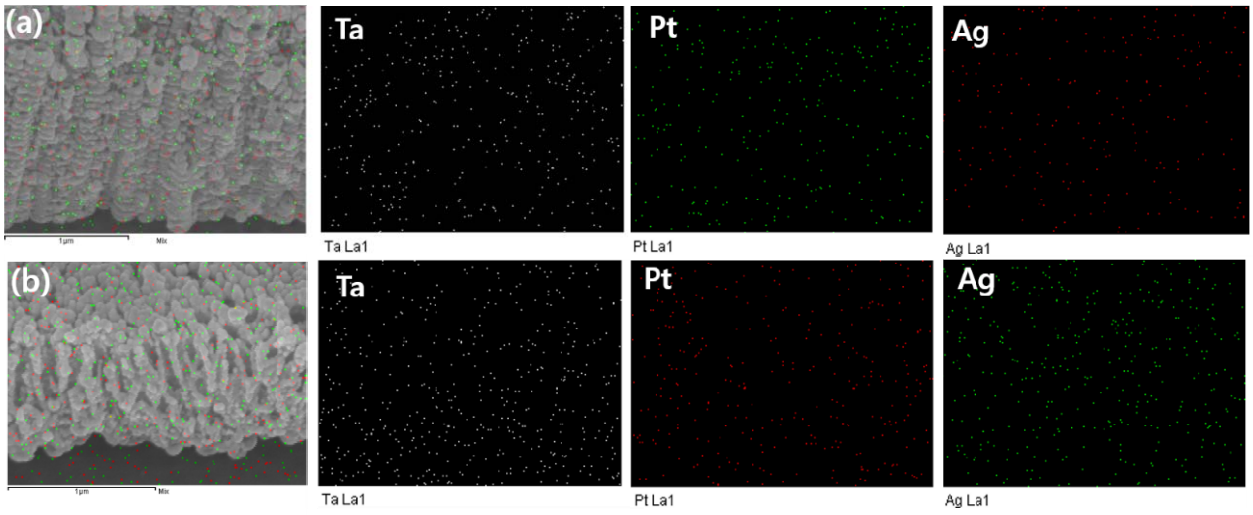

Figure 10. EDS mapping analysis results of the cross-section of the nanotube layers formed : (a) Ti-30Ta-2Ag-2Pt alloy and (b) Ti-50Ta-2Ag-2Pt alloy.

Table 4. EDS analysis results of nanotube formed Ti-xTa-2Ag-2Pt alloys.

Specimen / Elements (wt%)	Ti-10Ta-2Ag-2Pt			Ti-30Ta-2Ag-2Pt			Ti-50Ta-2Ag-2Pt		
	Surface	Bottom	Flaked	Surface	Bottom	Flaked	Surface	Bottom	Flaked
O	28.12	28.19	25.43	35.85	35.19	9.95	30.15	45.49	7.94
Ti	55.89	54.82	52.15	30.12	34.25	57.89	24.97	16.00	31.99
Ag	0.66	0.99	0.68	1.17	0.65	0.63	0.04	1.09	0.61
Ta	10.41	13.94	19.27	25.33	26.02	29.18	42.57	33.35	57.83
Pt	4.92	2.06	2.47	7.54	3.88	2.36	2.27	4.07	1.64
Total	100	100	100	100	100	100	100	100	100

Fig. 10 (b) is a cross-sectional image of Ti-50Ta-2Ag-2Pt alloy after nanotube formation. Fig. 10 (a) and (b) show that the Ta, Ag, and Pt ions are uniformly distributed. When Ag and Pt are excessively agglomerated on the TiO_2 nanotube, the bioactivity may deteriorate due to the electrochemical reaction in the mixed electrolyte. Therefore, excessive agglomeration must be prevented (28). Furthermore, the mapping distribution of Ag and Pt in Figure 10 (a) and (b) is well distributed in the nanotube layer, suggesting that the bioactivity performance is good. When the dental implant is implanted into the human body, it is expected to increase osseointegration and reduce healing time due to the antibacterial effect. The results of the EDS analysis after formation of the Ti-xTa-2Ag-2Pt alloy nanotubes are shown in Table 4. The EDS analysis results from the data are in good agreement with the EDS mapping results. As shown in Table 4, a certain amount of Ag and Pt were detected at the bottom portion of all the alloys near the substrate.

Fig. 11 shows the EDS mapping image of the surface of nanotube-formed Ti-xTa-2Ag-2Pt alloys in 1 M H_3PO_4 + 0.8 wt% NaF electrolytes for 2 h at an applied potential of 30 V. As shown in Fig. 10, it can be clearly confirmed that the Ta, Ag, and Pt ions are uniformly distributed over the entire surface of the alloy, which is thought to be helpful for cell adhesion and cell growth. In addition, nanotubes grown in β-type alloys are suitable for biomedical applications, as demonstrated by in vitro and in vivo testing (27).

Fig. 12 shows the XRD pattern of nanotube-formed Ti-xTa-2Ag-2Pt alloy with Ta content. The anatase phase of TiO_2 was detected at the peaks of all alloys and showed a strong peak tendency in Ti-30Ta-2Ag-2Pt alloy that was decreased in Ti-50Ta-2Ag-2Pt alloy. It seems to be the role of the Ta content, due to the formation of Ta_2O_5 film instead of TiO_2 film. The presence of the TiO_2 anatase phase on the titanium surface provides an advantageous environment favored by the cells (13). The anatase phase is more suitable for apatite formation than the rutile phase because of the crystallographic matching between the biomimetic apatite of the (0001) plane and the (110) plane for anatase is better than that between the biomimetic apatite of the (0001) plane and the (101) plane for rutile phase (29). As the Ta content increases, the peaks of Ta_2O_5 tend to increase gradually, as shown in Fig. 12.

Fig. 13 shows the result of the wettability test of the Ti-xTa-2Ag-2Pt alloy. Fig. 13 (a-c) shows the contact angle

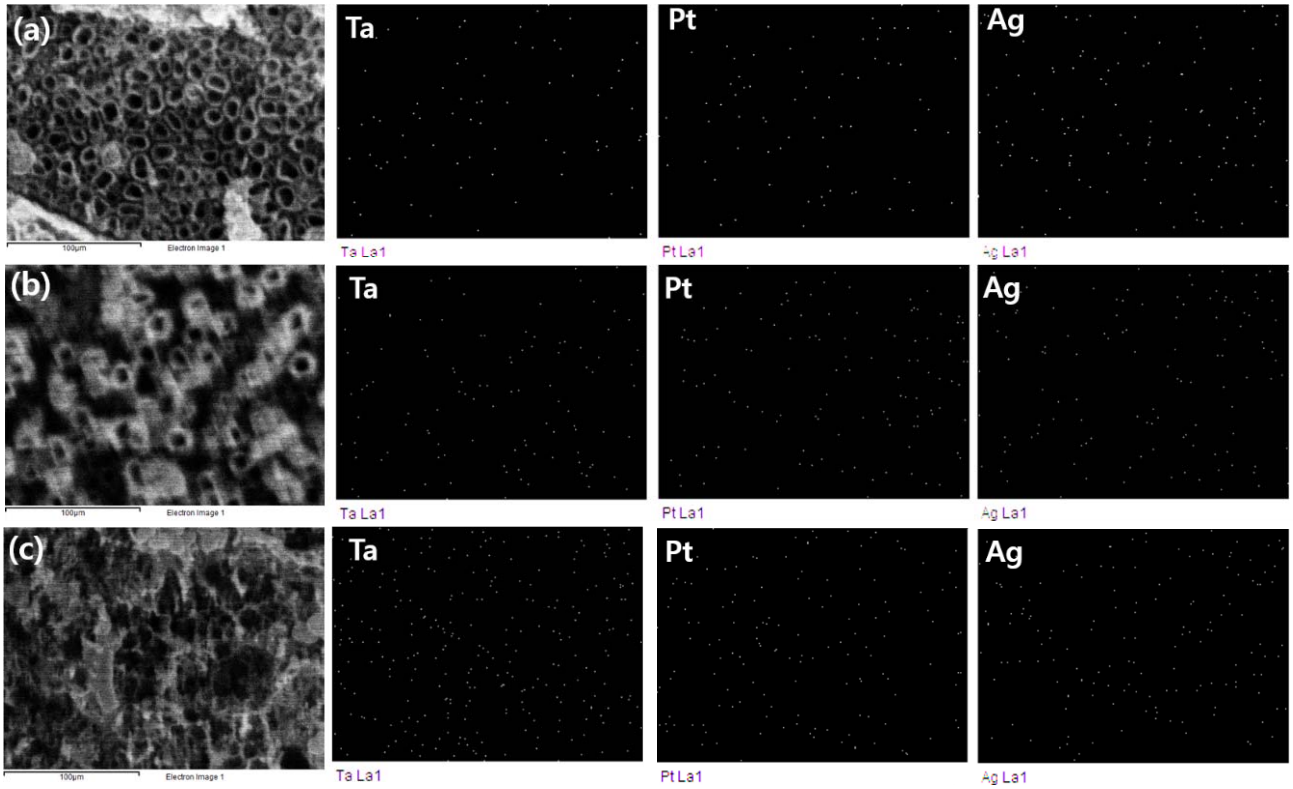

Figure 11. EDS mapping analysis results of the surface of the nanotube formed: (a) Ti-10Ta-2Ag-2Pt alloy, (b) Ti-30Ta-2Ag-2Pt alloy, and (c) Ti-30Ta-2Ag-2Pt alloy.

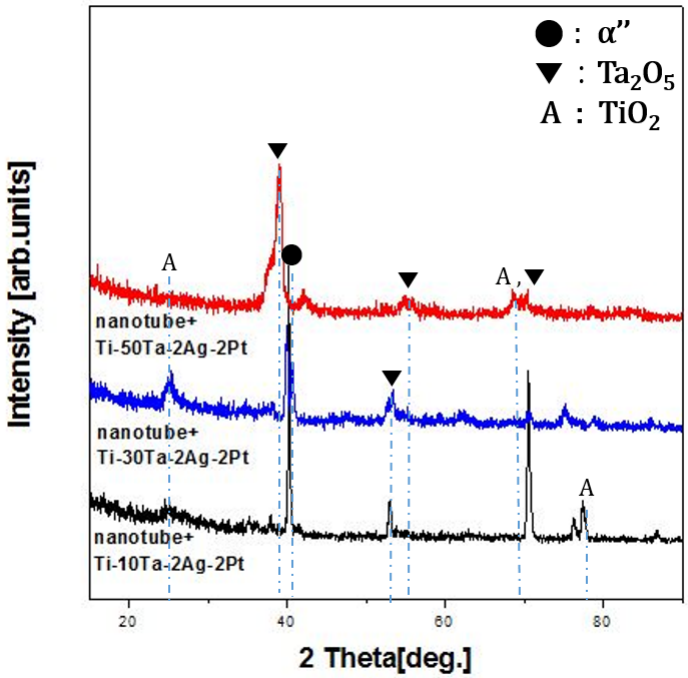

Figure 12. XRD patterns for the nanotube-formed Ti-xTa-2Ag-2Pt alloys.

of the Ti-xTa-2Ag-2Pt alloy on the surface of the etched microstructure. Fig. 13 (d–f) shows the contact angle of the Ti-xTa-2Ag-2Pt alloy to the surface after nanotube formation. Wettability can affect protein adsorption and activation, platelet adhesion, cell adhesion, and blood clotting. Furthermore, the surface wettability (hydrophilicity or hydrophobicity) determined through contact angle measurements is an important parameter affecting the biological response to the implanted biomaterial (30). In the case of the etched surface, the contact angles are (a) 62.10°, (b) 74.22°, and (c) 67.65°. The contact angle of the etched surface is slightly different due to the

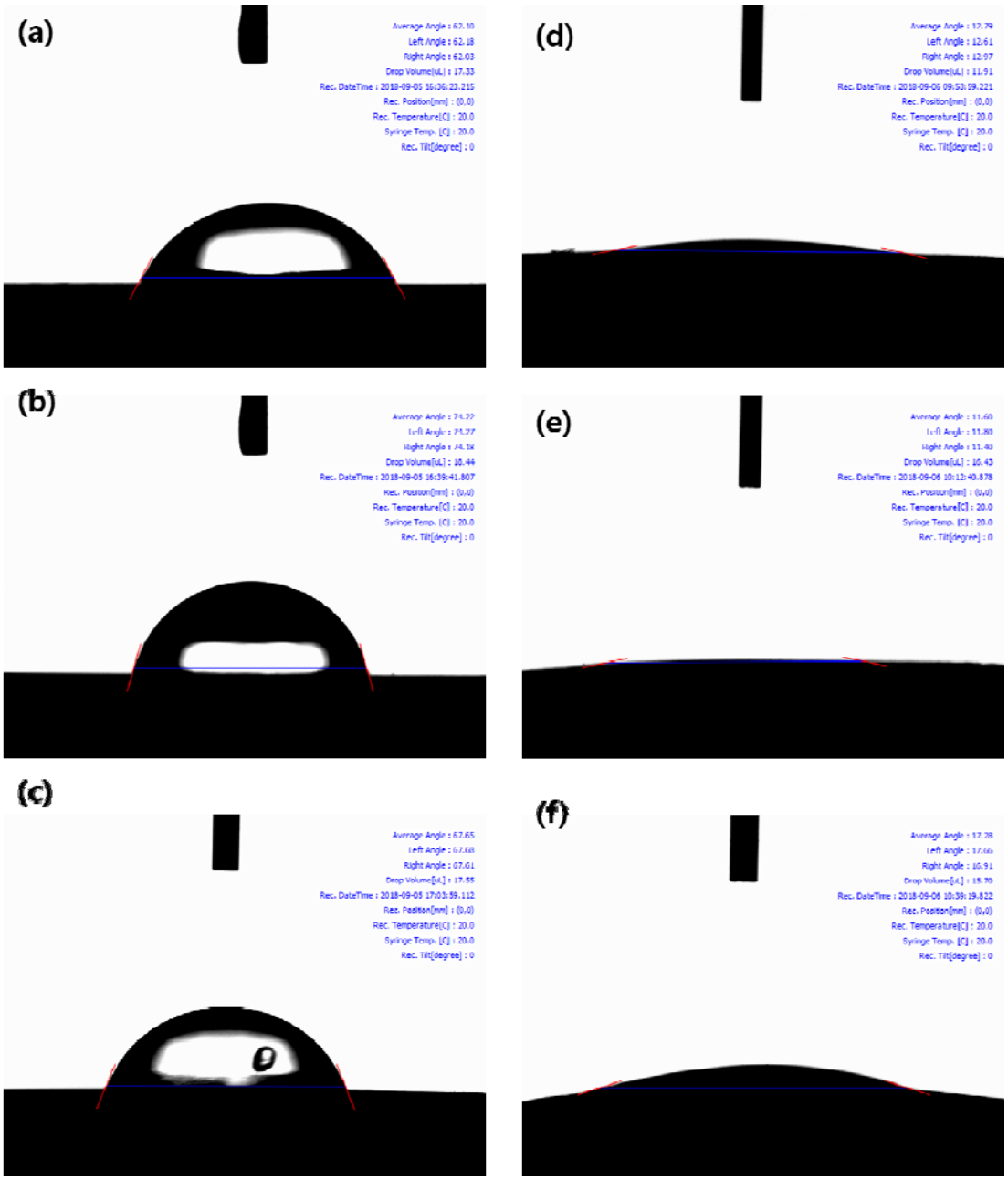

igure 13. Contact angles showing the Ti–xTa-2Ag-2Pt alloy surfaces: (a) etched Ti-10Ta-2Ag-2Pt, (b) etched Ti-30Ta-2Ag-2Pt, (c) etched Ti-50Ta-2Ag-2Pt, (d) nanotube formed Ti-10Ta-2Ag-2Pt, (e) nanotube formed Ti-30Ta-2Ag-2Pt, and (f) nanotube formed Ti-50Ta-2Ag-2Pt.

formation of needle-like and equiaxed structures with the variation in Ta content, as shown in Fig. 1. After the nanotube formation on the Ti-xTa-2Ag-2Pt alloy, the contact angles are (d) 12.79°, (e) 11.60°, and (f) 17.28°. In the case of the etched surface, the contact angle of the Ti-30Ta-2Ag-2Pt alloy was the highest, but the contact angle after nanotube formation was the lowest in the Ti-30Ta-2Ag-2Pt alloy. It is thought that wettability can be varied based on the influence of the size of two diameters, large and small, and microstructure of substrate as the Ta content increases. Therefore, it is considered that the surface with a low contact angle can be used for biomaterial implants because it has a close relationship with cell adhesion and can improve hydrophilicity as well as good cell adhesion and biocompatibility (24, 30).

Conclusions

The microstructure of the Ti-xTa alloy had an α"-phase Widmanstätten structure and a β-phase equiaxed structure, whereas Ti-xTa-2Ag-2Pt alloy showed properties similar to those of the Ti-xTa alloy. The β-phase and α-phase peaks were detected at all peaks. The thickness of the needle-like structure may be thinned by the addition of Ag and Pt. As the Ta content increased, the α-phase peak decreased and the β-phase peak increased. The Ti-30Ta-2Ag-2Pt alloy was shifted to the right, and its elastic modulus was lower than that of other alloys. The elastic modulus of the Ti-xTa-2Ag-2Pt alloy is much lower than that of the conventional CP Ti and Ti-6Al-4V alloys. The highly ordered nanotubes were formed in the Ti-10Ta-2Ag-2Pt and Ti-30Ta-2Ag-2Pt alloys, whereas the Ti-50Ta-2Ag-2Pt alloy formed nanoparticles. The diameters of the large and small nanotubes increased and decreased, respectively, with increasing Ta content. Ta, Ag, and Pt are uniformly distributed on the nanotube layer. Nanotubes did not grow in a needle-like structure (Widmanstätten), and nanotubes are not formed at the grain boundaries by fluoride ions, and the grain boundaries are heavily corroded, especially at the edges. The anatase phase of TiO_2 was detected at the peaks of all alloys and showed a strong peak tendency in Ti-30Ta-2Ag-2Pt alloy, whereas anatase peak was decreased in Ti-50Ta-2Ag-2Pt alloy. In the case of the etched surface, the contact angle of the Ti-30Ta-2Ag-2Pt alloy was higher than that after the nanotube formation.

Acknowledgement

This research was supported by NRF : 2016R1D1A1B 01016542

References

1. Liu R, Tang Y, Zeng L, Zhao Y, Ma Z, Sun Z, et al. In vitro and in vivo studies of anti-bacterial copper-bearing titanium alloy for dental application. Dental Mater. 2018;34(8):1112-26.
2. Cordeiro J, Faverani L, Grandini C, Rangel E, Cruz N, junior F, et al. Characterization of chemically treated Ti-Zr system alloys for dental implant application. Mater Sci Eng C. 2018;92:849-61.
3. Zhou YL, Niinomi M, Akahori T. Effects of Ta content on Young's modulus and tensile propertiesof binary Ti–Ta alloys for biomedical applications. Mater Sci Eng A. 2004;371(1-2):283-90.
4. Jeong YH, Kim WG, Choe HC, Brantley W. Control of nanotube shape and morphology on Ti–Nb(Ta)–Zr alloys by varying anodizing potential. Thin solid films. 2014;572:105-12.
5. Lei Z, Zhang H, Zhang E, You J, Ma X, Bai X. Antibacterial activities and biocompatibilities of Ti-Ag alloys prepared by spark plasma sintering and acid

etching. Mater Sci Eng C. 2018;92:121-31.
6. Ou SF, Wang CY. Fabrication of a hydroxyapatite-containing coating on Ti-Ta alloy by electrical discharge coating and hydrothermal treatment. Surf Coat Technol. 2016;302:238-43.
7. Mareci D, Chelariu R, Gordin DM, Ungureanu G, Gloriant T. Comparative corrosion study of Ti-Ta alloys for dental applications. Acta Biomater. 2009;5(9): 3625-39.
8. Chen M, Yang L, Zhang L, Han Y, Lu Z, Qin G, et al. Effect of nano/micro-Ag compound particles on the bio-corrosion, antibacterial properties and cell biocompatibility of Ti-Ag alloys. Mater Sci Eng C. 2017; 75:906-17.
9. Dowling DP, Betts AJ, Pope C, Connell ML, Eloy R, Arnaud MN. Anti-bacterial silver coatings exhibiting enhanced activity through the addition of platinum. Surf Coat Technol 2003;163-4:637-640.
10. Byeon IS, Hwang IJ, Choe HC, Brantley W. Electrochemically-coated hydroxyapatite films on nanotubular Ti-Nb alloys prepared in solutions containing Ca, P, and Zn ions. Thin Solid Films. 2016; 620:132-8.
11. Lakshmi B, Patrissi C, Martin C. Sol-Gel template synthesis of semiconductor oxide micro and nano-structures. Chem Mater. 1997;9(11):2544-25.
12. Macak JM, Sirotna K, Schmuki P. Self-organized porous titanium oxide prepared in Na_2SO_4/NaF electrolytes. Electrochim Acta. 2005;50(18):3679-84.
13. Park SY, Choe HC. Variations of nanotubes on the Ti-Nb-Hf alloys with applied voltages. Thin Solid Films. 2016;620:119-25.
14. Jo CI, Jeong YH, Choe HC, Brantley W. Hydroxy-apatite precipitation on nanotubular films formed on Ti-6Al-4V alloy for biomedical applications. Thin Solid Films. 2013;549:135-40.
15. Nguyen P, Won DH, Kim BS, Jang YS, Nguyen T, Lee MH, et al. The effect of two-step surface modification for Ti-Ta-Mo-Zr alloys on bone regeneration: An evaluation using calvarial defect on rat model. Apple Surf Sci. 2018;442630-9.
16. Oh KT, Shim HM, Kim KN. Properties of Titanium-Silver Alloys for Dental Application. J Biomed Mater Res. 2005;74(1):649-58.
17. Betts AJ, Dowling DP, McConnell ML, Pope C. The influence of platinum on the performance of silver-platinum anti-bacterial coatings. Mater Des. 2005;26(3): 217-22.
18. Tsuchiya H, Akaki T, Nakata J, Terada D, Tsuji N, Koizumi Y, et al. Anodic oxide nanotube layers on Ti-Ta alloys: Substrate composition, microstructure and self-organization on two-size scales. Corrosion Science. 2009;51(7):1528-33.
19. Gordin DM, Delvat E, Chelariu R, Ungureanu G, Besse M, Laille D, et al. Characterization of Ti-Ta alloys synthesized by cold crucible levitation melting. Adv Eng Mater. 2008;10(8):714-9.
20. Hwang MJ, Park EJ, Moon WJ, Song HJ, Park YJ. Characterization of passive layers formed on Ti-10 wt% (Ag, Au, Pd, or Pt) binary alloys and their effects on galvanic corrosion. Corrosion Science. 2015;96: 152-9.
21. Wei TY, Huang JC, Chao CY, Wei LL, Tsai MT, Chen YH. Microstructure and elastic modulus evolution of TiTaNb alloys. J Mech Behav Biomed. 2018;86:224-31.
22. Lee YT, Welsch G. Young's modulus and damping of Ti-6Al-4V alloy as a function of heat treatment and oxygen concentration. Mater Sci Eng A. 1990;128(1): 77-89.
23. Banerjee S, Mukhopadhyay P. Phase transformations, Examples from titanium and zirconium alloys. 1th ed. Oxford: Elsevier Science; 2007.
24. Kim ES, Jeong YH, Choe HC, Brantley W. Formation of titanium dioxide nanotubes on Ti-30Nb-xTa alloys by anodizing. Thin Solid Films. 2016;549:141-6.
25. Kim HJ, Jeong YH, Choe HC, Brantley W. Surface

characteristics of hydroxyapatite coatings on nanotubular Ti–25Ta–xZr alloys prepared by electrochemical deposition. Surf Coat Technol. 2014;259:274-80.
26. Choe HC, Kim WG, Jeong YH. Surface characteristics of HA coated Ti-30Ta-xZr and Ti-30Nb-xZr alloys after nanotube formation. Surf CoatTechnol. 2010;205: S305-11.
27. Luz AR, Souze GB, Lepienski CM, Siqueira CM. Tribological properties of nanotubes grown on Ti-35Nb alloy by anodization. Thin Solid Films, 2018; 660:529-37.
28. Jang JM, Chung SW, Choe HC, Brantley W. Electrochemical deposition behavior and characterization of Pd-Ag-HAp nanoparticles on ultra-fine TiO_2 nanotubes. Surf Coat Technol. 2017;320:383-90.
29. Wang Y, Yu H, Chen C, Zhao Z. Review of the biocompatibility of micro-arc oxidation coated titanium alloys. Mater Des. 2015;85:640-52.
30. Park SY, Choe HC, Effects of Hf content on nanotubular structure of Ti-29Nb-xHf ternary alloys. Surf Coat Technol. 2017;320:109-17.

Original Article

Surface characteristics of nanotube-formed Ti-Ta-Ag-Pt alloys for dental implants

*Seung-Pyo Kim, Han-Cheol Choe**

Advanced Functional Surface & Biomaterials Research Lab, Department of Dental Materials & Research Center of Nano-Interface Activation for Biomaterials, College of Dentistry, Chosun University Gwangju, Republic of Korea

In this study, the surface characteristics of nanotube-formed Ti-Ta-Ag-Pt alloys for dental implants were studied using various experimental instruments. The Ti-xTa-2Ag-2Pt quaternary alloys were manufactured using a vacuum arc-melting furnace with varying Ta contents (10, 30, and 50 wt%) and then homogenized by heat treatment at 1050 ℃ for 1 h. The nanotube formation of Ti-xTa-2Ag-2Pt (x = 10–50 wt%) alloy was performed using a DC power source of 30 V in 1.0 M H_3PO_4 + 0.8 wt% NaF electrolyte solution. The surface characterization was performed using optical microscopy (OM), field-emission scanning electron microscopy (FE-SEM), energy-dispersive X-ray spectroscopy (EDS), X-ray diffraction (XRD), and wettability and nano-indentation tests. The microstructure of the Ti-xTa alloy was composed of an α"-phase (Widmanstätten structure) and a β-phase equiaxed structure. The XRD peak of the α phase became weaker and that of the β phase became stronger with increasing Ta content. The elastic modulus of Ti-30Ta-2Ag-2Pt alloy was lower than those of the other alloys. The highly ordered nanotubes were formed in the Ti-10Ta-2Ag-2Pt and Ti-30Ta-2Ag-2Pt alloys; nanoparticles were found in the Ti-50Ta-2Ag-2Pt alloy. The diameters of the large and small nanotubes increased and decreased, respectively, with increasing Ta content. Nanotubes did not grow in a needle-like structure (Widmanstätten), and nanotubes are not formed at the grain boundaries and edges. The anatase phase of TiO2 was detected in Ti-30Ta-2Ag-2Pt alloy and disappeared in Ti-50Ta-2Ag-2Pt alloy. The contact angle of the nanotube-formed Ti-30Ta-2Ag-2Pt alloy was lower than those of the other alloys.

KeyWords : Ti-xTa-2Ag-2Pt alloys, Nanotube, Elastic modulus, α and β phase, Contact angle